Effect of Matrix Alignment and Substrate Stiffness on Migration of Heterogenous Myoferlin Depleted Breast Cancer Cell Populations

Yevgeniy Gladkiy

Department of Biomedical Engineering

College of Engineering

The Ohio State University

Columbus, OH

Spring 2019

Thesis Committee:

Dr. Samir Ghadiali, Advisor

Dr. Derek Hansford

Presented in Partial Fulfillment of the Requirements for Graduation with Honors Research Distinction in the Department of Biomedical Engineering at The Ohio State University

Abstract

Breast cancer is the second leading cause of cancer death in women (NBCF, 2019). Of all potential breast cancers, 10-20% are triple negative, which tend to be more aggressive than other breast cancer types ("Breastcancer.org - Breast Cancer Information and Support," 2019). Aggressive breast cancer is defined by the cancers ability to metastasize and spread to other parts of the breast. Myoferlin (MYOF), a protein that promotes cell motility and plasma membrane repair is reported at higher levels in breast cancer cells compared to normal tissue and previous studies by our group have observed the effect of removing or knocking down MYOF (MYOF-KD or KD) expression in the MDA-MB-231 cell line (Li et al., 2012). These studies indicated MYOFKD lead to Mesenchymal to Epithelial Transition (MET) in the MDA-MB-231 cells, leading to phenotypical and migratory changes promoting less aggressive behavior (Volakis et al., 2014). Although structural remodeling of the tumor microenvironment (TME) is known to facilitate cell migration, it is not known if these structural cues alter the migratory phenotype of MYOF-KD cells (Levental et al., 2009). Furthermore, it is not known how the presence of mixed cell populations (parental wild-type and MYOFKD) alters overall cell migration. Therefore, in this study we will investigate how structural cues and intercellular interactions between MYOFKD and parental wild-type (WT) cells influence cell migration behavior. For migratory experiments, patterned PDMS with rectilinear structure substrates will be prepared using soft lithography techniques. Additionally, aligned polyacrylamide gels were prepared with various stiffness. Cells will be labeled with lipophilic tracers to track migration with 24-hour time-lapse fluorescent microscopy. Cells will be seeded to form a rectangular monolayer or 3D tumor spheroids for migration.

Acknowledgements

I would like to thank Dr. Samir Ghadiali for providing me with the opportunity to conduct my undergraduate research project in his lab. He was an excellent advisor because of his ability to push me to work harder but continue to be friendly and understanding of my school work and extracurriculars. He provided me with an opportunity to work on COMSOL modeling through the STEP program and he provided invaluable guidance and aid for my first BMES conference.

I would like to thank Dr. Vasudha Shukla for her guidance in and out of the research project. She has been the most important foundation in this project because of her knowledge and flexibility. I am very grateful as she always encouraged me to explore throughout this project. This has taught me about the immense amount of effort it takes to complete research work.

I would also like to thank everyone in Ghadiali lab at this moment, Chris, Youjin, Justo, Tricia, Basia, Qinqin and Grant. The lab experience and environment would not be the same without this amazing group of people.

I would like to thank The Ohio State College of Engineering and The Ohio State Undergraduate Research Office for providing funding. I would also like to thank my friends who were interested in hearing about my work and even came to my oral defense.

Most importantly I would like to thank my family, who have been supportive financially and emotionally throughout my undergraduate career. Without them, I do not think I could have achieved as much as I have now.

Table of Contents

List of Figures

List of Tables

Chapter 1 : Background

1.1 Breast Cancer

Breast cancer is the second leading cause of cancer mortality in women (NBCF, 2019), and most deaths are caused by metastasis (@NCICancerStats, 2019). In situ breast cancer most commonly occurs in the parenchymal tissue which includes lobular carcinoma and ductal carcinoma ("Breastcancer.org - Breast Cancer Information and Support," 2019). The lobules are glands that are responsible for milk production and the ducts connect the lobules to the nipple. Breast stromal tissue is made up of adipose tissue, extracellular matrix (ECM), fibroblasts, lymph and blood vasculature. As seen in Figure 1-1, healthy tissue is highly structured and segregated, while cancerous tissue is shown to be an unorganized mesh of carcinoma and stroma.

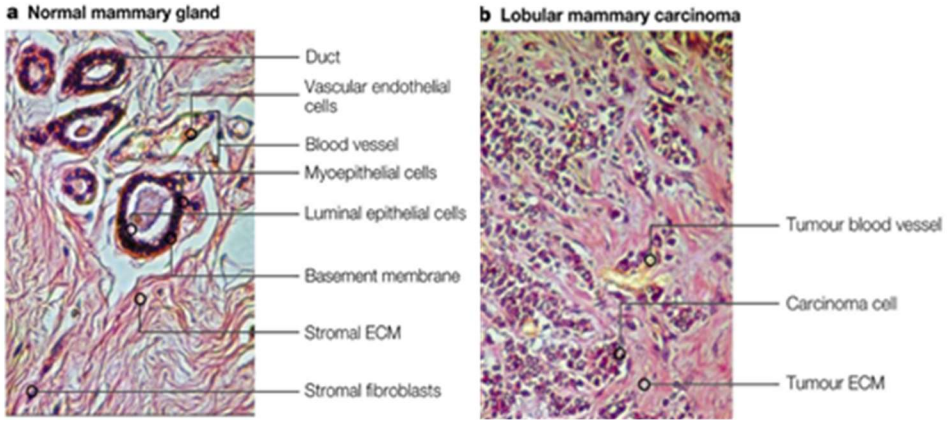

Figure 1-1: Comparison of healthy mammary gland tissue to mammary carcinoma. Normal mammary gland has a well-organized structure, while the carcinoma exhibits (Bissell & Radisky, 2001).

About 80% of breast cancers show invasive behavior, meaning the cancer has begun to grow into surrounding breast tissue or metastasize to distant organs and lymph nodes ("Breastcancer.org - Breast Cancer Information and Support," 2019). Triple negative breast cancer (TNBC) is considered significantly more invasive and has a poor short-term prognosis (Bianchini, Balko, Mayer, Sanders, & Gianni, 2016). TNBC is defined by tumors that do not

respond to hormonal therapies that target the estrogen receptor (ER), progesterone receptor (PR), and human epidermal growth factor receptor 2 (HER2) (Bianchini et al., 2016). Since there is a lack of known bio-markers, TNBC treatment is dependent on cytotoxic chemotherapy (Bianchini et al., 2016), and almost all women with metastatic TNBC will not survive (Bonotto et al., 2014) Therefore, alternative approaches towards preventing breast carcinoma metastasis should be studied.

1.2 Stromal Activation

Components of the tumor stroma or tumor microenvironment (TME) include the fibroblasts, immune cells, endothelial cells and the extracellular matrix (ECM). The TME acts as a "wounds that does not heal" because it replicates the granulation tissue of wounds and mimics the recruitment of macrophages, fibroblasts and blood vessels under chronic inflammation (Dvorak, Flier, & Underhill, 2009).

ECM remodeling is a core component of tumor malignancy and metastasis, which causes over 90% of deaths from cancer (Cox & Erler, 2011). The tumor ECM is composed of increased collagen deposition, collagen crosslinking, and glycosaminoglycan (GAG) glycoproteins content such as hyaluronan. It provides structural support and has a role in providing contextual information to control cellular behavior (chemotaxis, mechanotaxis, durotaxis). The composition of the ECM is dependent on the location in the body, for example there is a higher concentration of secreted protein acidic and rich in cysteine (SPARC) in bone to promote bone mineralization (Termine, Belcourt, Conn, & Kleinman, 1981). Additionally, ECM composition can be modulated by internal and external stimuli, for example impairment of movement decreases bone density, and exercise increases it (Rittweger et al., 2009). The extracellular basement membrane (BM) is responsible for maintaining epithelial polarity and structural support (Bilder, Li, &

Perrimon, 2000). Changes in the BM can lead to loss of polarity, which can directly lead to increased proliferation and tumorigenesis (Bilder et al., 2000).

A major component of the TME are fibroblasts, which were first defined as cell in the connective tissue that made collagen (Kalluri, 2016). Activated fibroblasts, in context of wound healing were identified by the greater expression of molecular markers such as alpha smooth muscle actin (α-SMA). Figure 1-2 shows the difference in levels of α-SMA in normal and tumor stroma.

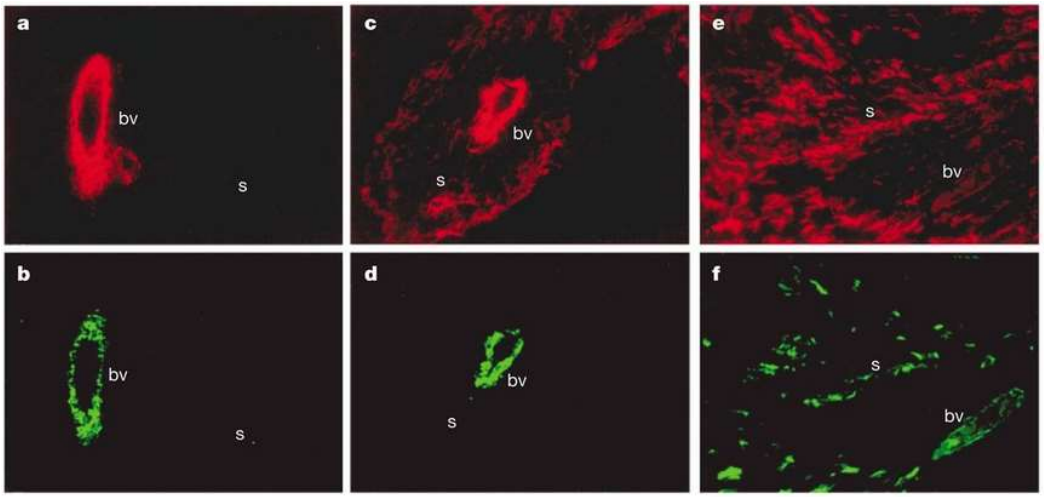

Figure 1-2: Differences of stroma between normal and breast tumor tissue. a. Shows no smooth muscle actin (in red) of normal stroma (s), and b. shows no smooth muscle myosin (green) in the stroma but does show strong staining of blood vessels (bv). In the tumor tissue, both c. and e. show high levels of a-SMA, but only f. shows positive for smooth muscle myosin (Rønnov-Jessen, Petersen, Koteliansky, & Bissell, 1995).

Myofibroblast generation is typically induced, such as with mechanical stimuli or with biochemical cues like transforming growth factor β (TGF-β) (Ronnov-Jessen & Petersen, 1993). Additionally, myofibroblast contraction can release TGF−β from the ECM of a stiff matrix present in granulation tissue (Wipff, Rifkin, Meister, & Hinz, 2007). In terms of cancer, activated fibroblasts are called cancer-associated fibroblasts (CAFs) because of an epigenetic change that retains the activated state. Studies with fibroblasts from human breast tumor have shown unique epigenetic changes that are not observed in normal mammary tissue (Hu et al., 2005). CAFs

promote invasion by generating ECM to guide cancer cells (Gaggioli et al., 2007). Activated fibroblasts also produce ECM degrading matrix metalloproteins (MMPs). Specifically, stromelysin-1 (MMP-3) is involved in the development of breast cancer because it cleaves E-cadherin and may perpetuate further epithelial to mesenchymal transition (EMT) (Sternlicht et al., 1999).

1.3 Epithelial to Mesenchymal Transition

EMT occurs when polarized cell undergo biochemical changes to assume mesenchymal phenotype. The loss of E-cadherin expression has been widely studied as a major factor that induces EMT because of its role in cell-cell adhesion (Kalluri & Weinberg, 2009). TGF-β suppresses epithelial cell proliferation, but in cancer cells the pathway is mutated and promotes EMT (Flanders & Wakefield, 2009). TGF-β signals the induction of Snail, Slug, and SIP1, which repress the expression of E-cadherin (Peinado, Quintanilla, & Cano, 2003). EMT-activating transcription factors (EMT-TFs), such as SNAIL1, TWIST1 and ZEB1 have been identified as key factors inducing EMT (Brabletz, Kalluri, Nieto, & Weinberg, 2018). But is not clear that these EMT-TFs play similar roles, as results of deleting different EMT-TFs are conflicting in the role of metastasis (Brabletz et al., 2018). An interesting behavior of mesenchymal to epithelial transmission (MET) happens when a tumor metastasizes to a secondary site as shown in Figure 1-3 (Zeisberg, Shah, & Kalluri, 2005).

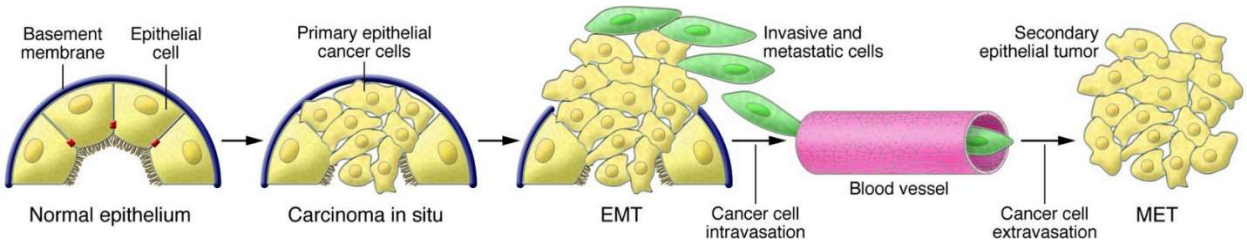

Figure 1-3: Epithelial to mesenchymal transition leads to metastasis. Epithelial cells lose their polarity and the basement membrane degrades allowing for invasion. These cells begin the process of intravasation where they metastasize to a secondary size and begin MET (Kalluri & Weinberg, 2009).

1.4 Matrix Stiffness

The elastic modulus of normal breast tissue has an elastic modulus of 0.4 – 2kPa while cancerous breast tissue is around 4-12kPa (Yu, Mouw, & Weaver, 2011). Increasing matrix stiffness by increasing collagen concentration has shown to enhance Rho-generated cytoskeletal tension to promote focal adhesion (FA) assembly and increase growth-factor-dependent ERK activation while decreasing stiffness normalized behavior (Paszek et al., 2005). Interestingly there is no change in adhesion strength, but the size of adhesion was greater on the stiff matrix (Paszek et al., 2005). The stiffening of a mammary gland as it transitions to a tumor shows the linearization and reorientation of collagen adjacent to the tumor seen in Figure 1-4 (Levental et al., 2009). Stiffening and remodeling of the ECM was accounted by collagen crosslinking, which promoted focal adhesions and therefore increased invasiveness (Levental et al., 2009). Though substrate stiffness is known to increase migration, it is not sufficient on its own to induce EMT (Shukla, Higuita-Castro, Nana-Sinkam, & Ghadiali, 2016).

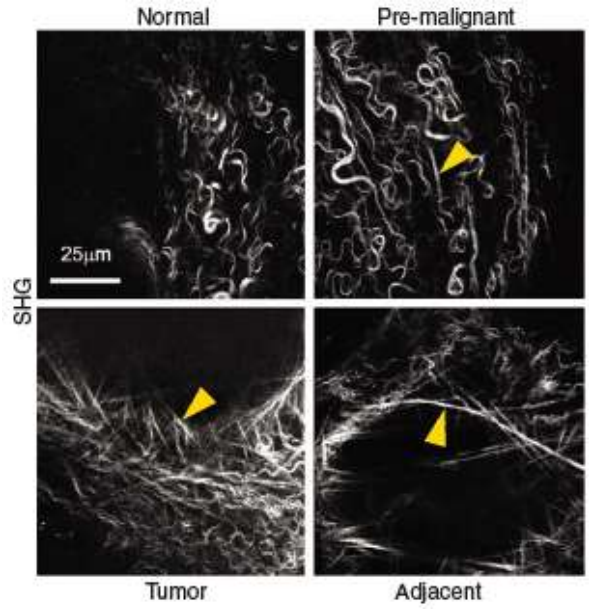

Figure 1-4: Collagen alignment in carcinoma progression. Shows mammary gland of mice with activated neu oncogene driven by a tumor virus promoter. Using second harmonic generation imaging, it is seen that collagen networks increase linearity with malignancy, which increases tissue stiffness (Levental et al., 2009)

1.5 Significance of Myoferlin

Previous studies have shown that Myoferlin (MYOF), a protein part of the ferlin family that promotes cell motility, vesicle trafficking and plasma membrane repair is reported at higher levels in breast cancer cells compared to normal tissue (Li et al., 2012). The FER-1 (Fertilization defective-1) was discovered in *Caenorhabditis elegans*, where loss of FER-1 resulted in loss of migration and vesicle fusion in *C.elegans* sperm cells (Argon & Ward, 1980). Mutations of ferlin proteins in human patients have been found to cause defects in cell membrane repair and vesicle fusion leading to muscular dystrophy and deafness (Bansal & Campbell, 2004; Roux et al., 2006).

Previous studies from Ghadiali group selected the use of highly invasive MDA-MB-231 due to the high level of MYOF expression (Li et al., 2012). Examination of mRNA expression in multiple cell lines showed lowered expression of MYOF in MCF-10A (a non-cancerous mammary tissue), MCF-7 and T47D (both non/low-invasive breast cancers). While BT549 and MDA-MB-231 (triple-negative and highly invasive breast cancers) showed a 2.44-fold higher expression of MYOF(Li et al., 2012). A wild-type parental cell line (WT) was used to knock down (KD) the expression of myoferlin (MYOF) using lentiviral mediated delivery of short hairpin ribonucleic acids (shRNAs). Additionally, a lentiviral control (LVC) was created using a non-human gene targeting construct. A comparison in morphology between KD, LVC and WT seen in Figure 1-5, showed that KD cells exhibited a more epithelial-like morphology compared to the LVC. KD maintained a clustering behavior compared to LVC. LVC were elongated with small and directional lamellipodia and short filopodia, actin filaments were oriented with the elongated axis. MYOF had broad single lamellipodia and numerous long filopodia. These results were confirmed quantitatively by another study done in Ghadiali group seen in

Figure 1-6 (Volakis et al., 2014). MYOF depletion was not found to affect the proliferation rate by testing KD and LVC cell lines with an MTS assay and a cell cycle analysis (Li et al., 2012). To confirm if knocking down MYOF promoted MET, markers of EMT expression were tested by immunoblotting. KD expressed higher levels of epithelial marker E-cadherin and lower levels of mesenchymal markers fibronectin and vimentin, which confirmed MET in KD cells.

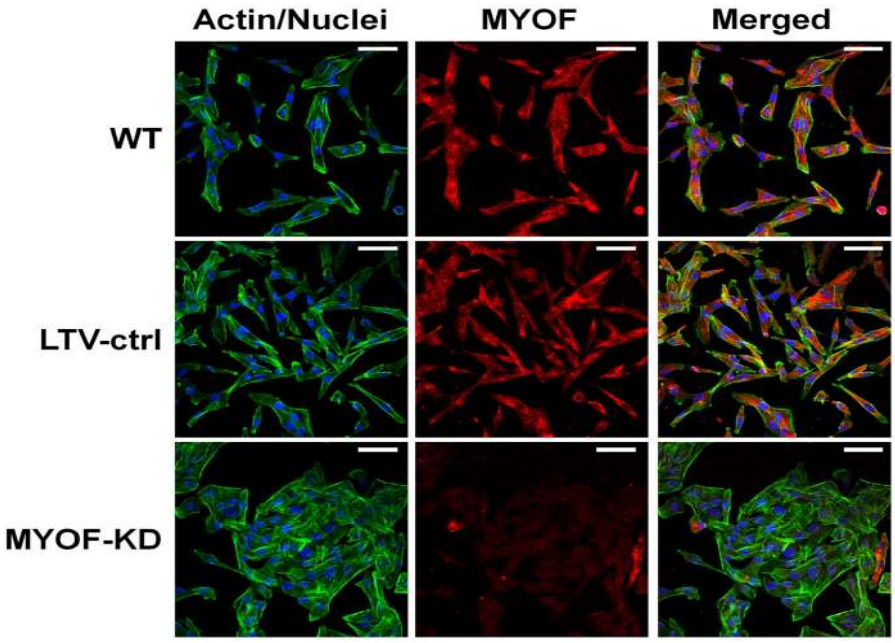

Figure 1-5: Myoferlin depleted MDA-MB-231 morphology. Shows immunofluorescent images of the morphological differences of myoferlin depleted cells which resemble an epithelial shape compared to the mesenchymal lenti-viral control and wildtype (Li et al., 2012).

The relative adhesion strength of WT, KD and LVC cell lines were testing using a novel assay that measured the transcellular impedance developed by Ghadiali group. Results indicate that the loss of MYOF significantly increased relative adhesion strength and spreading adhesion strength (Volakis et al., 2014). Atomic force microscopy (AFM) imaging was performed to show how MYOF depletion affected the cytoskeletal frame of MDA-MB-231 cells. The LVC cells showed an elongated morphology with elongated actin stress fiber formation while KD cells were rounded with fewer actin stress fibers as seen in Figure 1-7.

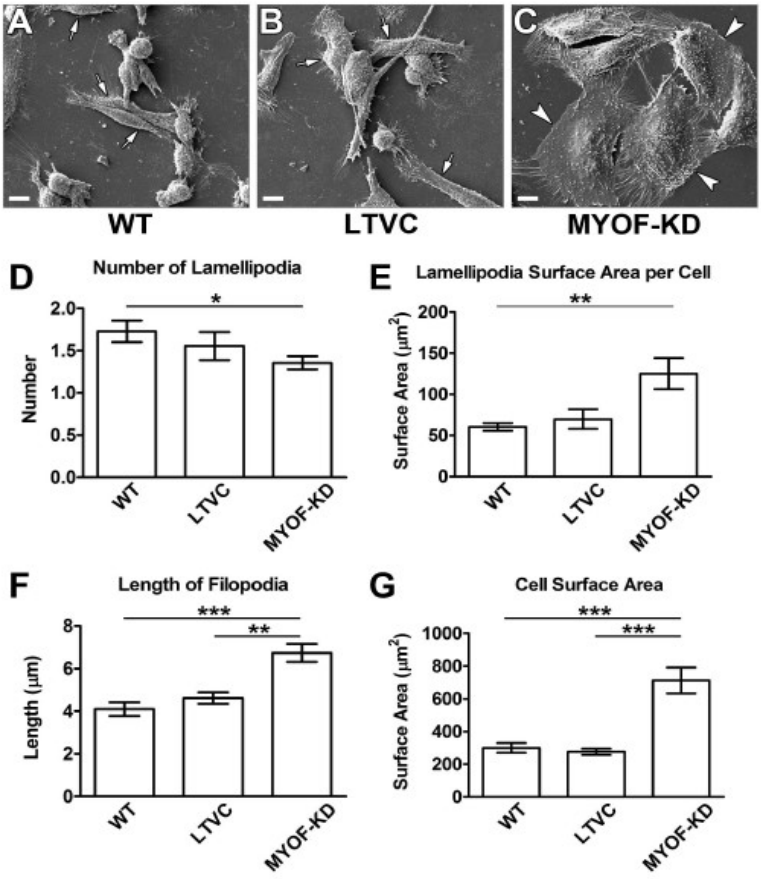

Figure 1-6: Myoferlin Depleted MDA-MB-231 shows increased surface area. SEM images of (A) WT, (B) LVC and (C) KD show the difference in morphology. A quantified confirmation of the difference in morphology is seen D-G (* $p<0.05$, ** $p<0.01$, *** $p<0.001$)(Volakis et al., 2014).

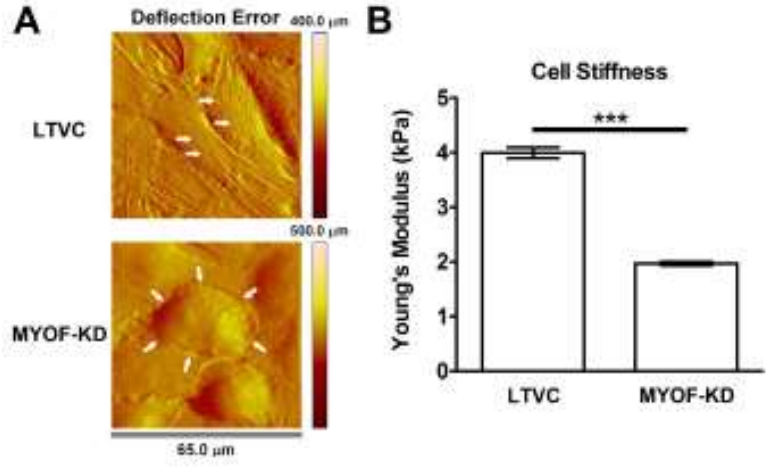

Figure 1-7: MYOF-KD causes a more deformable cell and less stress actin. AFM images confirmed elongated stress actin formation in LVC, while KD showed a more rounded formation (A). LVC were also found to be a stiffer cell (B) (*** $p<0.001$) (Volakis et al., 2014).

Additionally, KD cells exhibited a statistically significant decrease in Young's modulus compared to LVC. Traction force microscopy (TFM) indicated that KD exerted a consistent and lower traction stress compared to LVC which had a larger range (Volakis et al., 2014). Boyden Chamber assays with 10% FBS used as a chemoattractant showed no difference in migratory behavior indicating no difference in chemotaxis (Li et al., 2012). But when a Matrigel (reconstituted cell membrane) was introduced to the assay, there was a significant reduction in invasion for KD cells. Additionally, there was a statistically significant reduction in MMP1 secretion of KD, therefore when collagen I was used in the invasion assay, there was an even greater reduction when invasion assay. In Figure 1-8A, LVC cells exhibited significant cell-cell detachment and had random/non-directional migration while closing the wound gap. KD cells maintained a cohesive monolayer while close the wound gap, moving in a directional, sheet-like fashion mimicking the migration pattern of epithelial cells but showed a slower velocity. Figure 1-8E shows the progression of wound closure for LVC and KD cells. Other studies by Ghadiali group have shown that the addition of TGF-β1 to KD cells can increase velocity and decrease directionality and additionality induce EMT (Barnhouse et al., 2018). Additionally, migration on flat polyacrylamide gels of varying stiffness have been studied by Ghadiali group (Watts & Ghadiali, 2017). On 0.5 kPa gels, LVC seemed to migrate slower initially than KD cells, but eventually began to migrate at the same rate after 24 hours, but no statistical significance was found between the migratory patterns. On 2kPa gels, LVC cells were found to significantly travel more at some time points than KD, and similar results were found on 20 kPa gels.

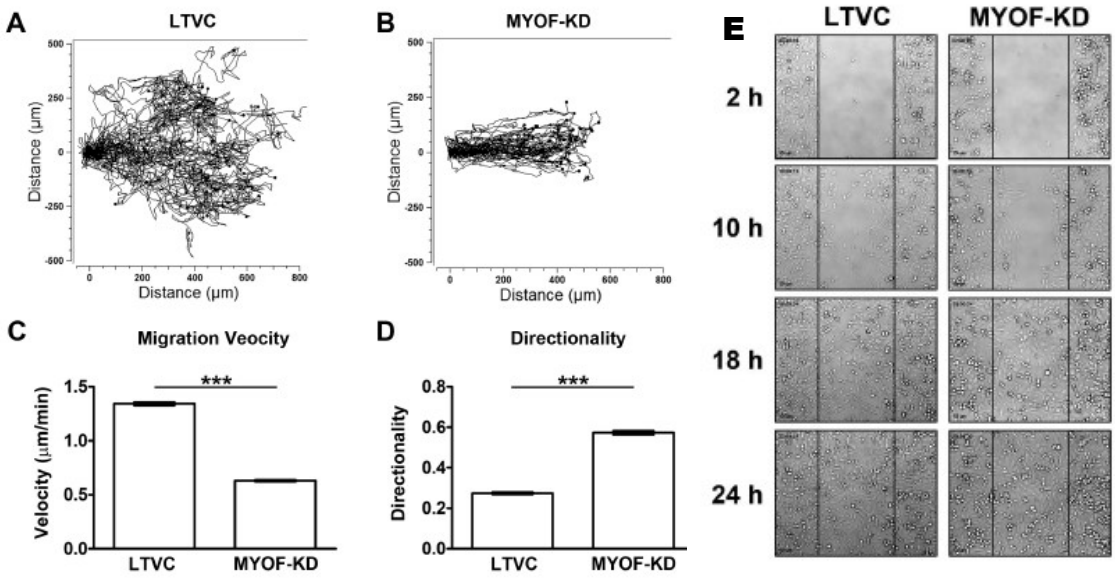

Figure 1-8: MYOF depletion lowers migration velocity but increases directionality.and (B) show a visualized pattern of migration, where LVC is more chaotic. (C) proves that velocity in KD cells is lower but directionality is increased (D). (E) represents the Ibidi wound assay that shows both LVC and KD achieved wound closure after 24 hours (Volakis et al., 2014).

Although structural remodeling of the tumor microenvironment (TME) is known to facilitate cell migration, it is not known if these structural cues alter the migratory phenotype of MYOF-KD cells (Levental et al., 2009). Furthermore, it is not known how the presence of mixed cell populations (WT and MYOF-KD) alters overall cell migration. Therefore, in this study we will investigate how structural cues and intercellular interactions between MYOFKD and parental wild-type (WT) cells influence cell migration behavior.

Chapter 2 : Materials and Methods

2.1 Cell Culture

The triple negative breast cancer (TNBC) MDA-MB-231 (ATCC, HTB-26) cell lines (gifted by Dr. Douglas Kniss) were used in this study. A wild-type parental cell line (WT) was used to knock down (KD) the expression of myoferlin (MYOF) using lentiviral mediated delivery of short hairpin ribonucleic acids (shRNAs) (Li et al., 2012). Additionally, a lentiviral control (LVC) was created using a non-human gene targeting construct. Each cell line was incubated (37°C, 5% CO_2, 95% humidity) in high glucose (4.5 g/L) Dulbecco's Modified Eagle Medium (DMEM) supplemented with 10% fetal bovine serum (FBS) and 5% Antibiotic/Antimycotic (Anti/Anti).

2.2 Spheroid Culture

LVC, KD, WT and mixed population (MX), with a 1:1 ratio of WT to KD, cell lines were prepared into clusters (10µL, 2000 cells) suspended in high glucose DMEM with 10% FBS and 5% Anti/Anti using the hanging drop method. The cell culture dish (60 mm x 15 mm), made with a layer of polydimethylsiloxane (PDMS) on the lid (10:1, polymer: crosslinker), was used to incubate the clusters for 48 hours (37°C, 5% CO_2, 95% humidity) before seeding. Droplets were placed with a pipet onto the surface of the PDMS layer of the lid, then the lid was inverted and placed onto the base filled with 2 mL of Phosphate-buffered saline (PBS) for incubation.

2.3 Lipophilic Labeling

For mixed population experiments, WT and KD were individually labeled with DiL and DiO (Fisher Scientific) lipophilic tracers respectively. Each cell line ($1x10^6$ cells/ 1mL) was spun

down (1500 rpm, 5 min) and resuspended with 1mL of serum free DMEM in a 1.5 mL conical tube. Each cell line was mixed with 10 µL of lipophilic tracer, spun and resuspended two more times with serum free media. Lastly, each cell line was spun and resuspended with 1mL high glucose DMEM with 10% FBS and 5% Anti/Anti for further use.

2.4 Aligned PDMS Mold

A SU-8 silicon wafer was produced using standard UV lithography (provided by Dr. Daniel Gallego-Perez), and used to mold a PDMS array (2 µm x 2 µm) with soft lithography techniques seen in Figure 2-1. The SU-8 wafer was placed in a 120 mm x 15 mm culture dish and premixed PDMS (25g polymer base, 2.5g crosslinker) was poured onto the SU-8 wafer. Once the PDMS was settled, the SU-8 wafer was pushed down to the culture dish bottom. The culture dish was placed into a vacuum desiccator and the PDMS mixture was degassed. Then the culture dish was placed in the oven (60^{o}C, 2hrs). The SU-8 wafer was carefully removed using a scalpel and excess unmolded PDMS was cut away. Then either a 15 mm hole punch was used for migration assay's or cut with a scalpel into 75 mm x 25 mm sections using a microscope slide as a stamp.

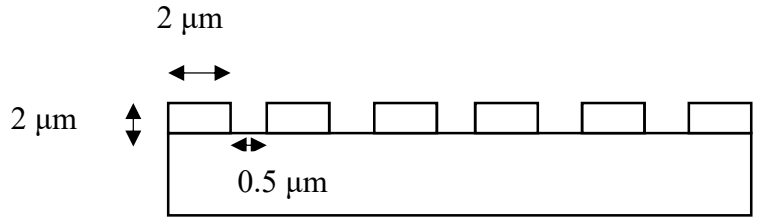

Figure 2-1: Representation of the PDMS Mold. PDMS was poured on a SU-8 wafer placed in a culture dish, desiccated, baked and cut out using a scalpel.

2.5 Aligned Polyacrylamide Gel Preparation

2.5.1 Coverslip Surface Modification

The 15 mm circular coverslips needed to be etched to allow proper bonding to polyacrylamide (PA). Initially the coverslips were washed with 70% EtOH, dried and then soaked in 0.1 M NaOH for 5 minutes. Then the coverslips were placed into an oven (55ºC, 1hrs) until dry. Then the coverslips were soaked in a 1:200 3-aminopropyltriethoxysilane (Sigma-Aldrich) solution for 30 minutes, soaked in deionized (DI) water for 5 minutes, washed individually with DI water and then dried. Next, the coverslips were soaked in 0.5% glutaraldehyde in PBS for 30 minutes, soaked in DI water for 5 minutes, rinsed with DI water and dried.

2.5.2 Polystyrene Sacrificial Mold

A new non-surface treated microscope slide was spin coated (1500 rpm, 1min) with 400 µL of 15% polystyrene (Sigma-Aldrich) in anisole (Sigma-Aldrich) and allowed to dry. A clean hot plate was heated to 175ºC, then the polystyrene (PS) covered glass slide was placed onto the hot plate (PS facing up) for 3 minutes. Next a fresh PDMS stamp was heated for 1 minute (pattern side facing up) and the stamp was carefully placed pattern side down onto the PS covered slide. Then using a stiff and hard object, the PDMS mold was pushed down with force for 3 minutes. After that, the glass slide with the PDMS mold was carefully removed from the hot plat and allowed to cool for 2 minutes. The PDMS mold was carefully peeled off, resulting in patterned PS that will be used to pattern a polyacrylamide (PA) gel seen in Figure 2-2. This protocol was provided by Dr. Hansford's lab (Miller & Hansford, 2018).

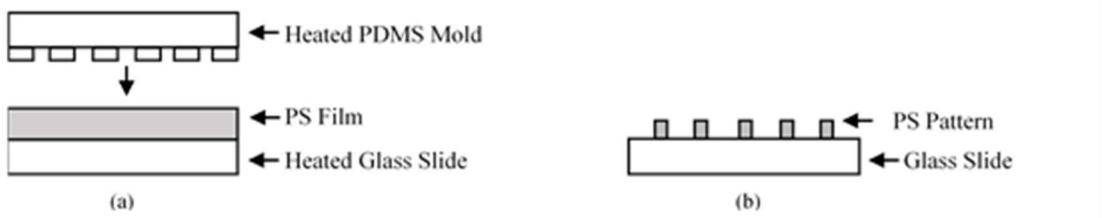

Figure 2-2: Steps of creating sacrificial polystyrene mold. The initial step of (a) uses a compression molding technique utilizing heated substrates that lead to the results (b).

2.5.3 Polyacrylamide Gel Mold

Polyacrylamide (PA) mixtures were prepared in separate 1.5 mL conical tubes. The following mixtures in Table 2-1 (Tse & Engler, 2010), used various amounts of acrylamide (Bio-Rad) and bis-acrylamide (Bio-Rad) in the table. 5 µl of 10 % ammonium persulfate (Sigma-Aldrich) and 0.5 µl of Tetramethylethylenediamine (Bio-Rad) were added to each mixture to initiate cross linking. 50 µL of PA gel solution was placed on the treated side of the 15 mm circular coverslips, and the coverslip was flipped onto the PS patterned glass slide. After 30-45 minutes, or when gel is seen to shrink, anisole was used to dissolve the PS pattern by washing and allowed the patterned PA gel to be easily separated. Then the gels were washed with DI water and stored in PBS until seeding.

Table 2-1: Polyacrylamide Gel Protocol. This Protocol is used to make 500 µL of each gel stiffness (Tse & Engler, 2010).

E (kPa)	Acrylamide (µL)	Bis -acrylamide (µL)	DI Water (µL)
0.5	37.5	15	447.5
2	50	25	425
20	100	66	334

2.5.4 Collagen Coating

The day of cell seeding, each PA gel was washed in sterile PBS. Next, 100 µL of 0.5 mg/ml of Sulfo Sanpah solution (Thermo Scientific) in HEPES buffer was placed on each gel, treated under UV light for 5 minutes then washed in sterile PBS. After this was done twice, each gel was placed in a 60 mm x 15 mm cell culture dish filled with a 1:1000 solution of 200 µg/ml bovine collagen (Advanced BioMatrix) in 10 mM HCL for one hour. Each gel was then washed with sterile PBS and prior to seeding was washed with 75% EtOH, and again in sterile PBS.

2.6 Live Cell Imaging

A 12-well dish was placed in the incubation chamber of the live-cell imaging system (37°C, 5% CO2, 95% humidity) and images were captured every 10 minutes for 24 hours (Olympus Ix81). Each cell line was imaged using differential interference contrast microscopy (DIC), while the mixed populations used CY5 and FITC filter. Captured images were saved and visually inspected using SlideBook 6®.

2.7 Tracking Migration

Images were analyzed using ImageJ Manual Tracking to track the migration of 25 cells on the migration edge per experiment. The average velocity (V), average x-velocity (xV), directionality (D) and x-directionality (D_x) were calculated using the distance formula shown below in MATLAB®.

$$Distance = \sqrt{((x_n - x_{n-1}) * (1/u))^2 + ((y_n - y_{n-1}) * (1/u))^2} \quad (1)$$

Where n= the time point, x = the x-coordinate, y = the y-coordinate and u = 1.55 scale for the 10x objective, and .62 for the 4x objective. Each x-axis-based measurement was used to analyze

migration strictly in the x-direction and was calculated similarly as standard measurements. Directionality is the ratio of euclidian distance to accumulated distance, where euclidean distance is the distance from first to last position. This shows the ability of a cell to move in a linear fashion in a certain direction from D = 1 to D = 0 which indicates random motion.

2.8 Wound Assay

Cells at concentration of $3.0x10^5$ cells/mL in culture DMEM media were placed into each well of a wound assay insert (Ibidi) as seen in Figure 2-3. Each insert was individually placed in a 12-well plate where cells were incubated (37°C, 5% CO2, 95% humidity) for 24 hours so a confluent monolayer could form. The insert was removed and an additional 2 mL of culture DMEM was added to each well before live cell imaging. Four experiments were performed for LVC, KD, WT, and MX. Five cells were tracked per experiment for a total of n = 25 per cell line, KD and WT were individually tracked for mixed cell populations.

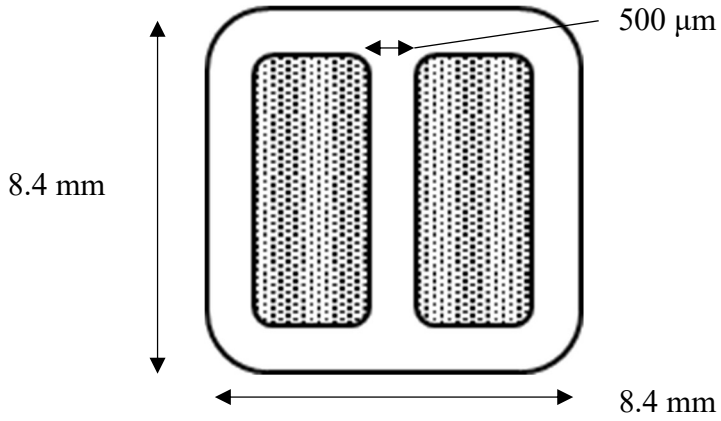

Figure 2-3: Wound assay insert for wound assay. The shaded portions of each side indicate cells being seeded in each well with a concentration of $3.0x10^5$ cells/mL.

2.9 Single Well Assay

The same procedures for seeding, incubation, live imaging and tracking were used as for wound assay. Three sets of four experiments for LVC, KD and MX were performed, with each set representing flat, PDMS parallel and perpendicular array migration represented in Figure 2-4.

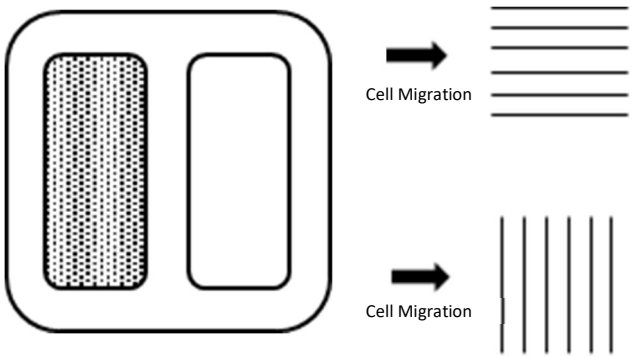

Figure 2-4: Use of insert with single front migration assay. Only one well was filled indicated by the shaded portion. But experiment were conducted on tissue culture plastic (flat), and PDMS arrays that were either perpendicular or parallel to the migratory front.

2.10 Cluster Assay

Spheroid cultured cells, from KD, LVC and mixed population were placed on flat and PDMS array surfaces contained in a 12 well plate. Spheroids were allowed to incubate for 3 hours to allow attachment, then wells were flooded with 2 mL of culture DMEM. Two sets of four experiments for LVC, KD, WT, and MX were performed with each set representing flat and array pattern. Five cells were tracked per experiment for a total of n = 25 per cell line, KD and WT were individually tracked for mixed cell populations. A same live imaging protocol was used as previously stated.

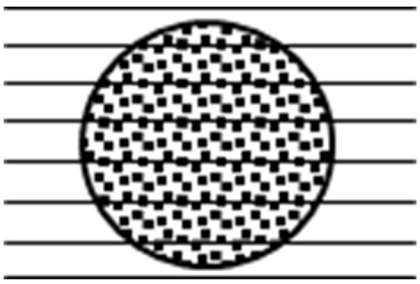

Figure 2-5: Use of insert with single front migration assay. Only one well was filled indicated by the shaded portion. But experiment were conducted on tissue culture plastic (flat), and PDMS arrays that were either perpendicular or parallel to the migratory front.

2.11 Aligned Polyacrylamide Gel Assay

Spheroid cultured cells from all cell lines (KD, WT, LVC) were individually placed on high (20 kPa), medium (2 kPa) and low (0.5 kPa) stiffness aligned gels. Figure from the cluster assay similarly represents the aligned gel assay, and the attachment protocol was the same as from the cluster assay. Each gel was secured to the bottom of the wells of the 12 well plate using sterile silicone grease placed on the edges of the 15 mm circular coverslip. Four experiments per cell line for the three gels were performed, where five cells were tracked per experiment for a total of n = 25 per cell line.

2.12 Statistical Analysis

The statistical analysis was performed in Sigma Plot v.14 (Systat). For each data set a Shapiro-Wilk normality and Brown-Forsythe equal variances test was performed with an a = 0.05. The data sets that had normality and equal variances established had results presented as mean +/- standard error, where significance was tested with a One-way ANOVA with $p \leq 0.05$ and the Tukey Test was used for *post hoc* analysis. Data sets where normality or equal variances test was not established, results were presented as median +/- standard deviation. The significance was test with a Kruskal-Wallis One Way ANOVA on Ranks with $p \leq 0.05$ and the Tukey Test was used for *post hoc* analysis.

Chapter 3 Results

3.1 Myoferlin Depletion of MDA-MB-231 Alters Wound Migration

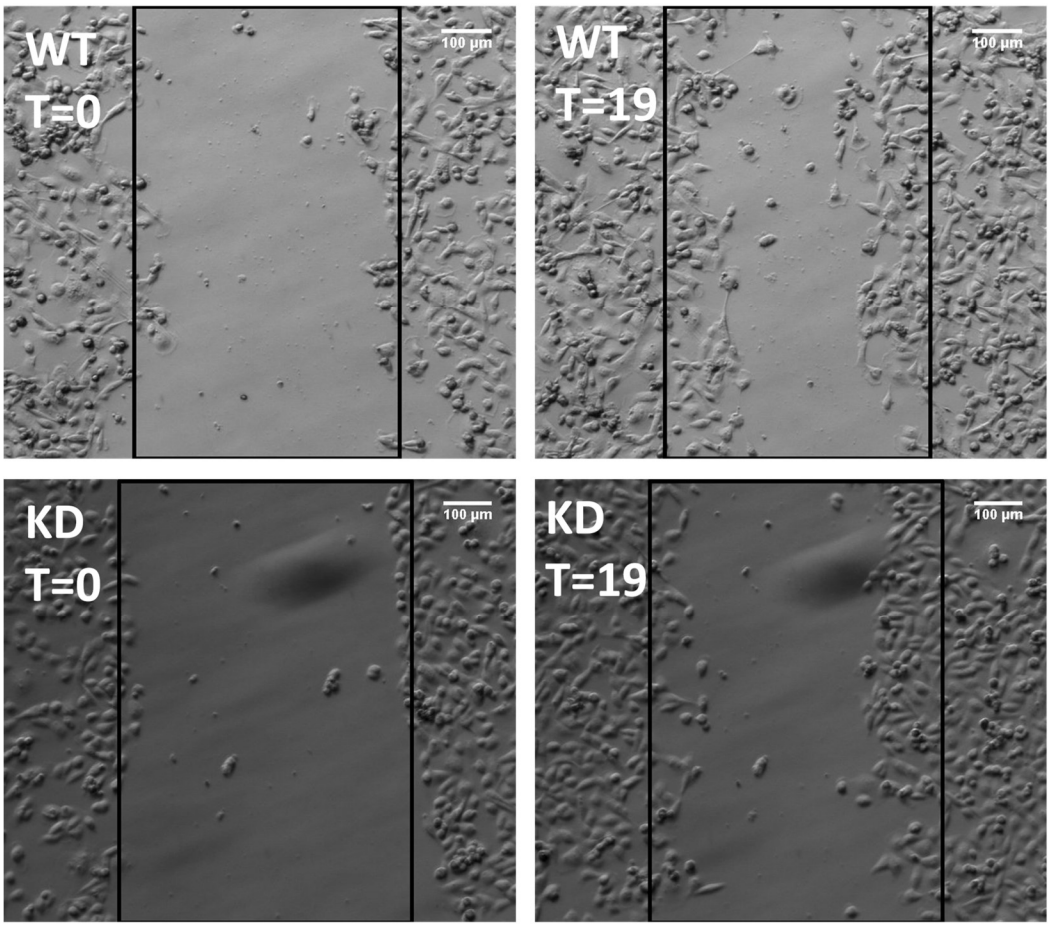

Figure 3-1: Wound closure of WT and KD cells. Differential interference contrast microscopy (DIC) time-lapse images of WT and KD cells taken during wound closure assay. A faster wound closure is seen for WT at 19 hours compared to KD but with more randomized movement. While KD cells follow a sheet like migration.

An Ibidi wound insert, live-cell imaging and tracking techniques were used to follow the migration of LVC, KD and WT cell lines. Cells were seeded into the wound assay chambers and grown until a confluent monolayer formed. Then the Ibidi was then removed, live-cell imaging was performed and then cells were individually tracked using ImageJ. In Figure 3-1, WT cells exhibit a greater wound closure, leading cells show an elongated shape reflecting a spindle-like shape and have more cells that are detached from the migration front. Not shown, LVC cells

showed a similar migration pattern. KD cells have a smaller wound closure, showing a flatter shape and greater cell-cell adhesion as seen by a cohesive epithelial like migration.

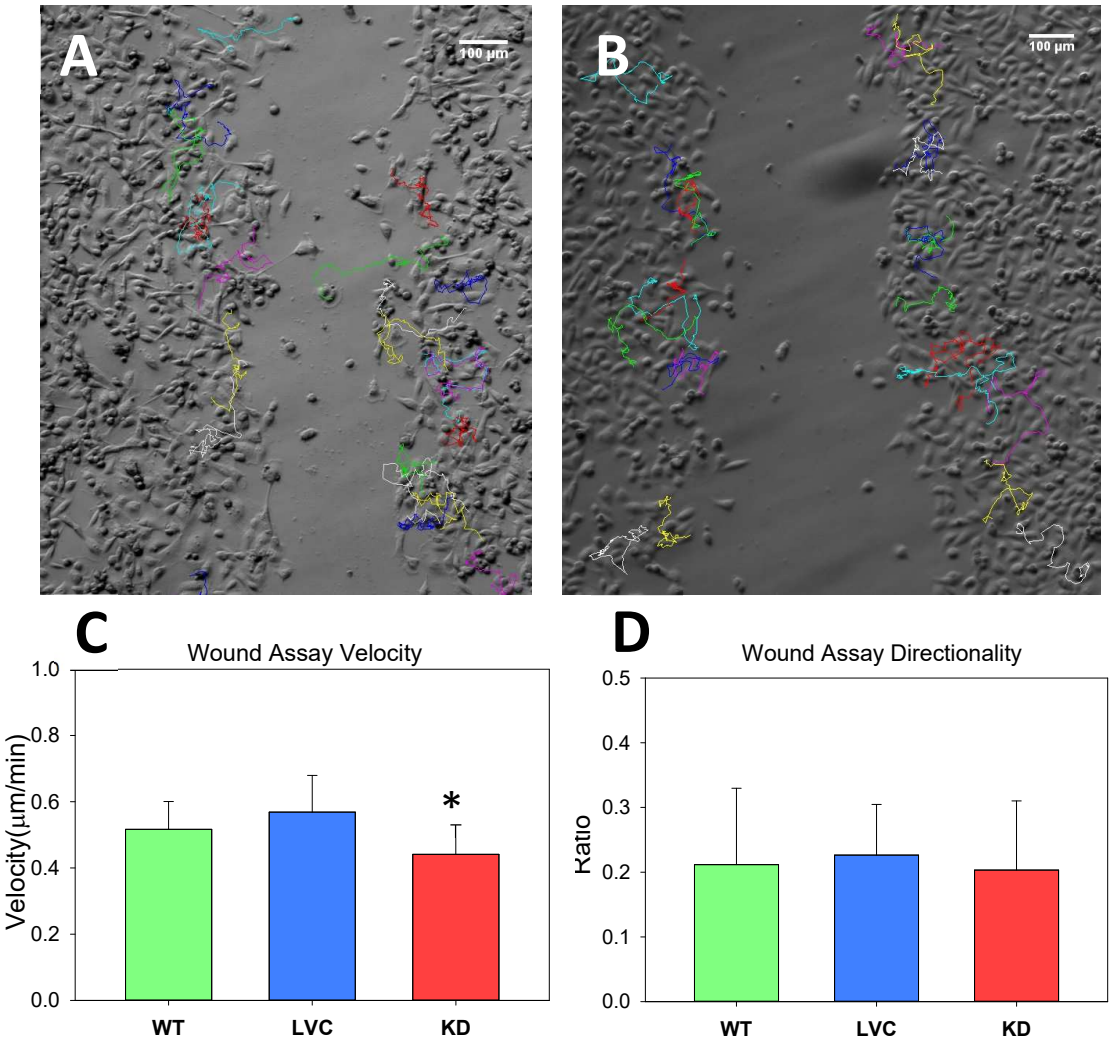

Figure 3-2: Myoferlin depletion causes lower velocity of migration. (A) shows the migratory patterns of WT cells which have random movement with less cell adhesion as opposed to the migratory pattern of KD (B). The velocity of KD is significantly lower than LVC and WT (C), but there is not difference in directionality (D) (* $p<0.05$).

In Figure 3-2, LVC cells have a greater tendency to break away from the migration front, show random movement but tend to move in parallel to the migratory front. KD cells did not show any leading migration that breaks away from the front and tend to move in a localized area. Quantitative analysis shown in Figure 3-2, shows that KD cells had a significantly lower velocity than WT and LVC cells. But directionality of each cell line did not significantly differ.

3.2 Heterogenous Cell Populations Negate the Effect of Myoferlin Depletion in Wound Migration

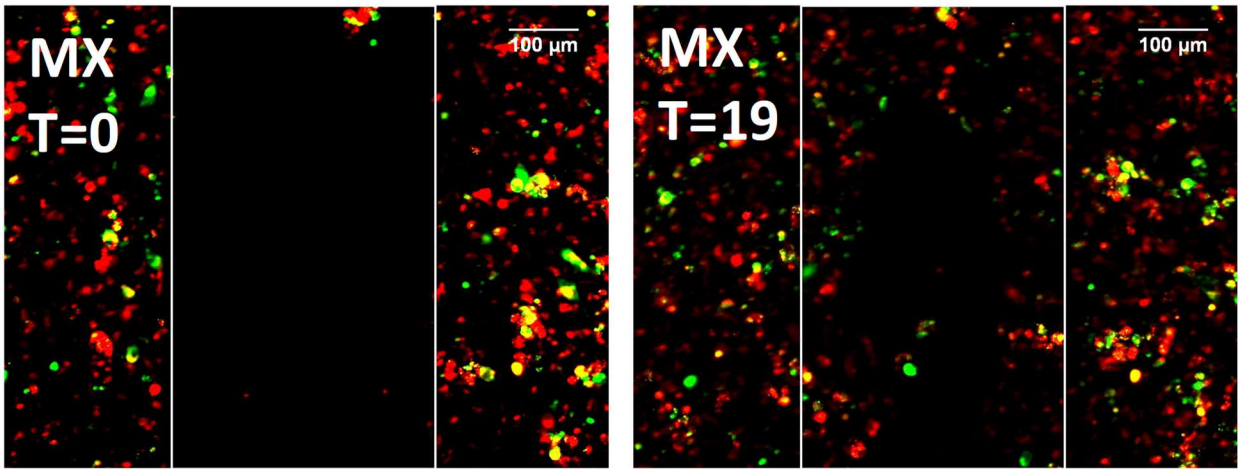

Figure 3-3: Wound closure of mixed cell populations. Red cells represent KD, while green cells represent WT. It is seen that KD cells continue to migrate in a epithelial fashion and have the WT cells act as the leading migration boundary.

This experiment was similarly prepared to the previous wound assay experiment but a 1:1 mixture of WT and KD cells that were labeled with lipophilic tracers. WT and KD cells were individual tracked to see if a heterogenous population would affect cell migration. Interestingly, it can be seen in Figure 3-3 that the wound closure was similar to WT only behavior. KD cells continued to migrate in an epithelial fashion and seemed to prevent WT cells from engaging in random movement, pushing the WT cells toward wound closure. Quantitative analysis in Figure 3-4 shows that velocity of KD significantly increased, and directionality of both WT and KD cells significantly increased as well.

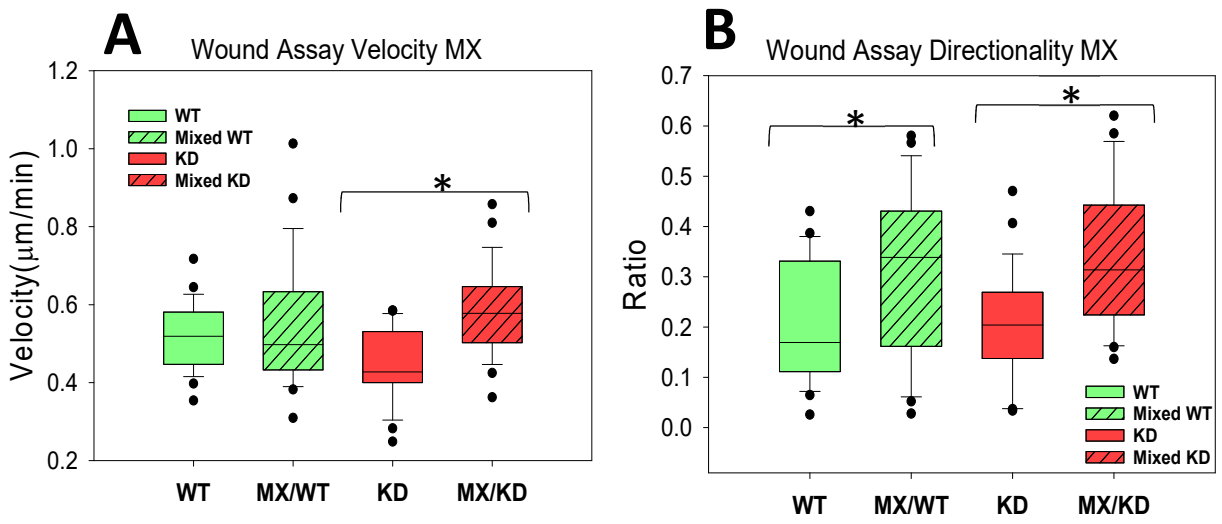

Figure 3-4: Heterogenous cell population alters wound migration in WT and KD cells. (A) shows that KD cells in the mixed cell population have a significant increase in velocity. (B) indicates a significant increase of directionality in both mixed WT and KD cells (* $p<0.05$).

3.3 Parallel and Perpendicular Arrays Alter Single Front Migration

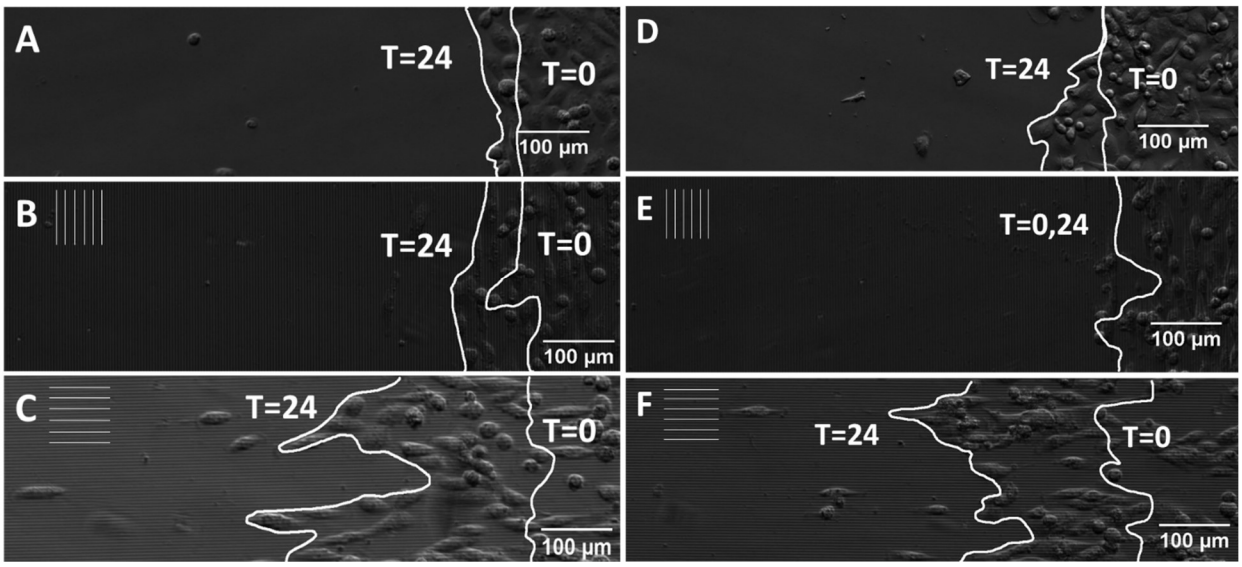

Figure 3-5: Single front migration experiments of LVC and KD. (A-C) show the migration of KD, where (A) is flat, (B) is parallel and (C) is perpendicular. (D-F) show the migration of LVC, (D) is flat, (E) is parallel and (F) is perpendicular.

This experiment was prepared using the Ibidi wound assay insert but only one well was utilized. The Ibidi was either placed on either tissue culture plastic (TCP) or on the PDMS array mold with the cell front oriented in parallel or perpendicular to the array. Figure 3-5A-C represents the KD cell line while 3-5D-F represent the LVC cell line. In Figure 3-5A, the

perpendicular PDMS arrays clearly show a greater migration distance of KD cells compared to parallel (3-5B) and flat (3-5A). Interestingly, the KD cells begin to show an elongated morphology representing a potential EMT. Additionally, there is a slightly more migratory behavior in the parallel array compared to the flat surface of the KD cells. Though there is less migration in the parallel array, KD cells still show an elongated cell structure in the direction of the array. In 3-5D, the LVC cells migrate a greater distance the KD cells on the flat surface. But unlike KD, the LVC cells to not migrate at all when a parallel array is present seen in 3-5E. There seems to be no difference between migratory distance of KD and LVC on perpendicular arrays.

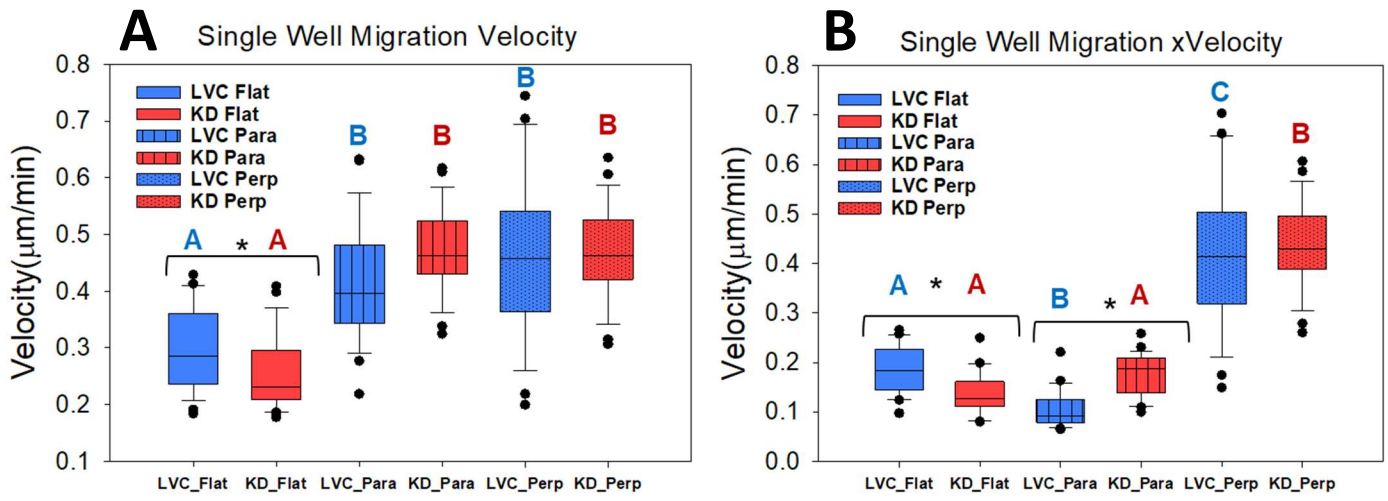

Figure 3-6: Analysis of velocity and x-velocity in single well migration experiment. Quantification of migratory behavior of KD and LVC on flat, perpendicular and parallel array surfaces(*p<0.05). (A) represents velocity and (B) represents the velocity in the x-direction. Blue letters relate to LVC and red letter relate to KD, where a difference in letter indicates statistical significance.

Figure 3-6A shows the velocity of migration of all single well migration experiments. Velocity accounts for overall cell movement in any direction. Between the three surface conditions that LVC cells migrated, there was a significant increase of velocity between the flat surface and both parallel and perpendicular array. But no difference was seen between each array for LVC. The KD cell line had the same results regarding the three surface conditions. When

comparing KD to LVC of each surface condition, the only significant difference was seen on the flat surface, where LVC cells migrated faster than KD. Figure 3-6B shows the x-axis velocity of all single well migration experiments. The velocity in the direction of the x-axis was chosen to see migratory differences given the preference of cells to move towards open space. Between the three surface conditions that LVC cells migrated, all three had significantly different outcomes, the fastest was the perpendicular array, then the flat surface and the slowest was the parallel array. Between the three surface conditions that KD cells migrated, perpendicular was the fastest while the parallel array and flat surface had no significant differences. When comparing KD to LVC of each surface condition, LVC were again faster on flat than KD. Interestingly, the KD cells were faster in the x-axis on the parallel array, while there was no difference on the perpendicular array.

3.4 Effect of Mixed Populations on Single Well Migration

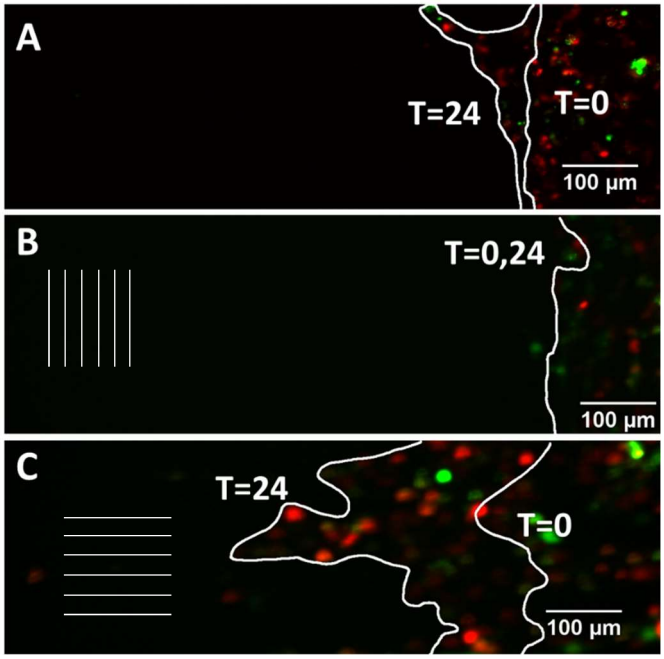

Figure 3-7: Single front experiments of mixed populations. Mixed populations of KD (red) and WT (green) were tested on flat (A), parallel (B) and perpendicular (C) surfaces.

This experiment was set up in the same fashion as described for the KD and LVC single front experiment. The KD are represented as red and WT is represented as green. Overall the migration patterns seen in Figure 3-7 showed a similarity to LVC. 3-7C is seen to have the largest migration distance on the perpendicular array. Then the flat surface has the next largest migration difference seen in 3-7A. Interestingly, it is clearly in 3-7A that there is a leading WT cell that promotes the migration of the KD cells lagging behind. For the parallel array in 3-7B, there is no visual evidence showing any migratory behavior.

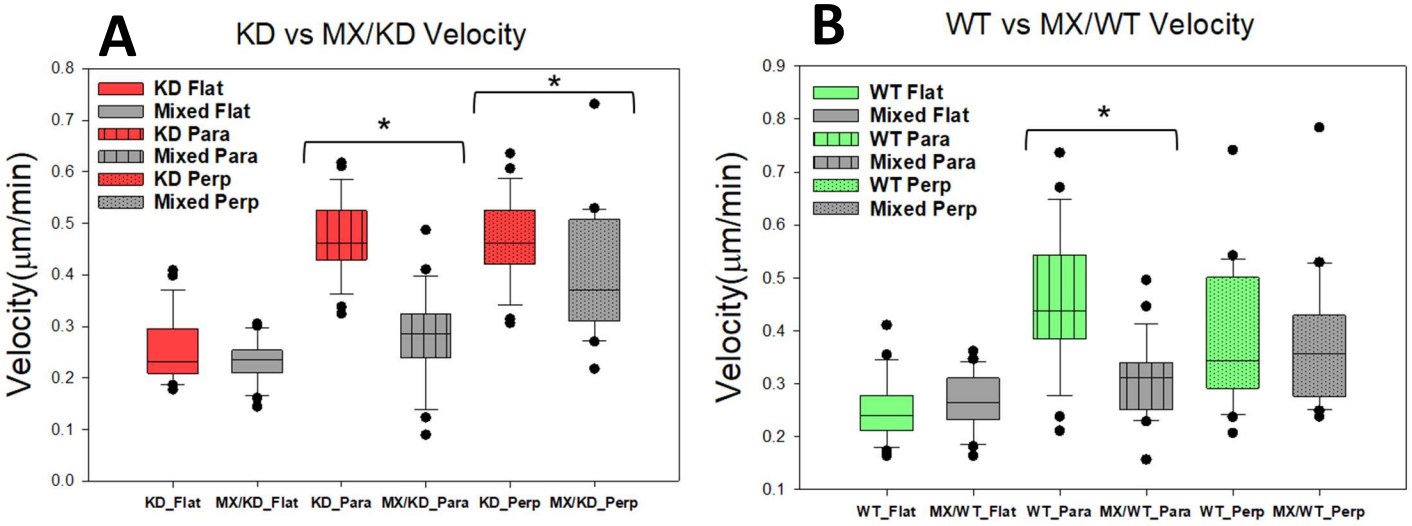

Figure 3-8: Quantified analysis of velocity comparing mixed populations to individual cell lines. (A) represents the analysis of KD to mixed KD populations, where only the same surface conditions were compared to each other. This was similarly done for WT seen in (B)(*$p<0.05$).

In 3-8A, there is a significant difference in the parallel array and perpendicular array surface condition for KD. The individual KD cell line on the parallel array is seen to migrate faster than the mixed population KD cells. Similarly, the KD only cells migrated significantly faster than the mixed population cells. In 3-8B, there is a significant difference only between the parallel array, where the isolated WT line is significantly faster than the mixed WT population.

3.5 Cluster Migration is Improved with Myoferlin Depletion and Array

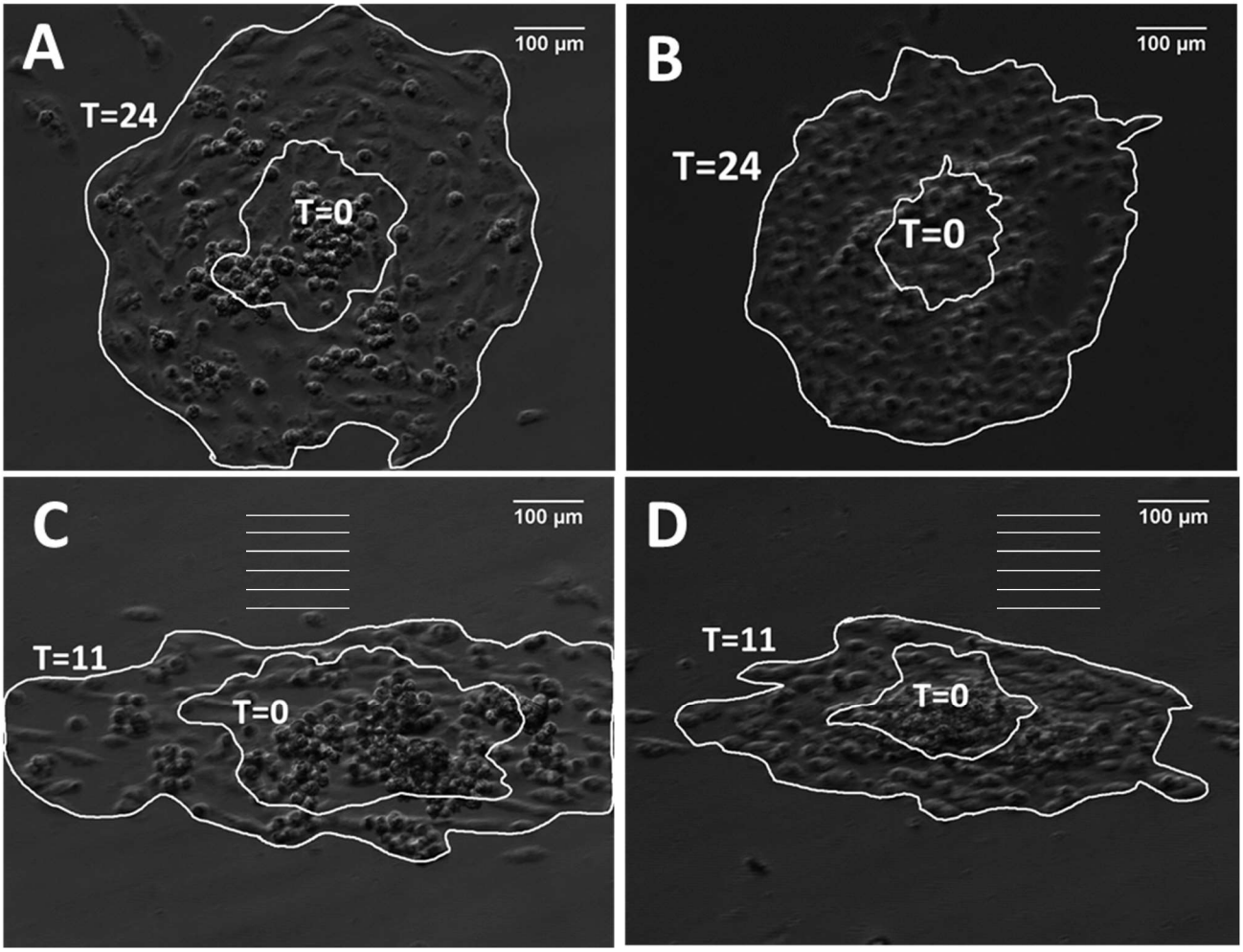

Figure 3-9: Cluster migration on flat and lined surfaces of KD and LVC. (A) and (C) represent KD on flat and lined surfaces respectively. (B) and (D) represent LVC on flat and lined surfaced respectively. The analysis time of the lined arrays was shorter to track fast moving cells going off frame.

Clusters of n=2000 for each cell line were seeded on TCP and PDMS arrays. Comparing the size of KD and LVC on flat surfaces on Figure 3.5A-B, it is seen that KD cells have a greater surface area over time than LVC. Additionally, KD cells show a more epithelial shape, as each individual cell is seen to be flatter and more spread out, while LVC cells are more rounded. In Figure3.5C-D, even after 11 hours, significant cellular spreading occurs, specifically in the

direction of the array pattern. Interestingly, there is greater cellular spreading in the KD than the LVC cells.

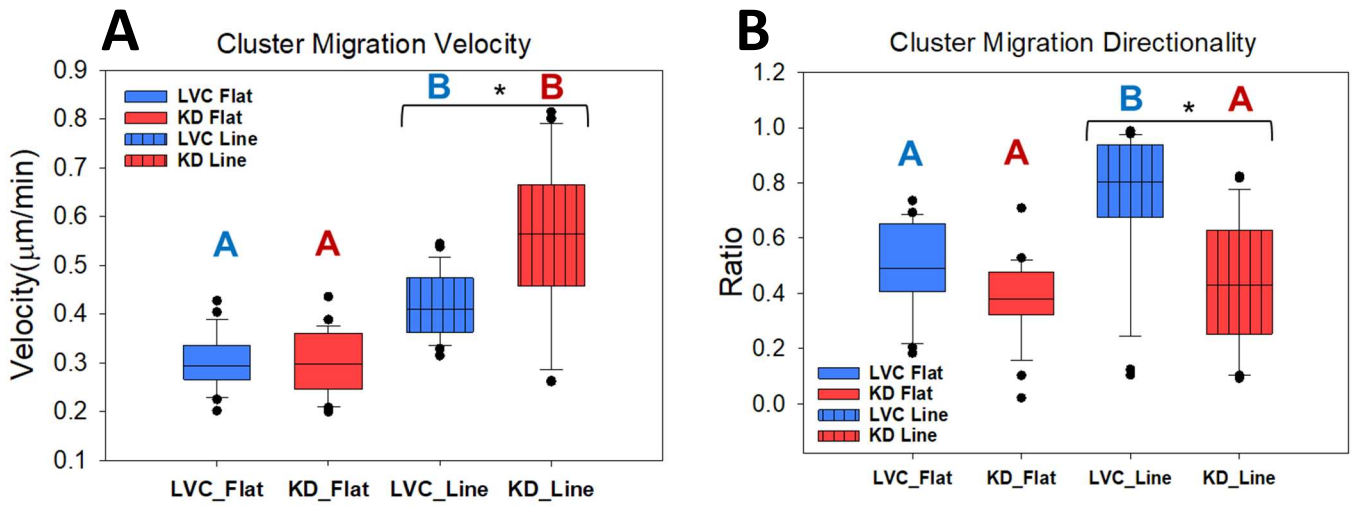

Figure 3-10: Quantitative analysis of LVC and KD cluster migration. Analysis of LVC and KD on flat and aligned PDMS arrays is represented as (A) velocity and (B) directionality. The statistical significance of * was $p<0.05$. The blue letters represent LVC and red represents KD, where a difference in letters shows statistical significance.

In Figure 3-10A, between the two surface conditions of LVC, the PDMS array significantly increased velocity. The same significant increased happened comparing flat and array of KD cells. But interestingly the velocity of KD cells was significantly greater than LVC. Figure 3-10B shows that there is a significant increase in LVC directionality when lines are introduced, while KD cells do not have a significant increase. Additionally, the LVC cells had a significantly greater directionality than the KD cells on the PDMS array.

3.6 Mixed Populations Significantly Lower Directionality in Clusters

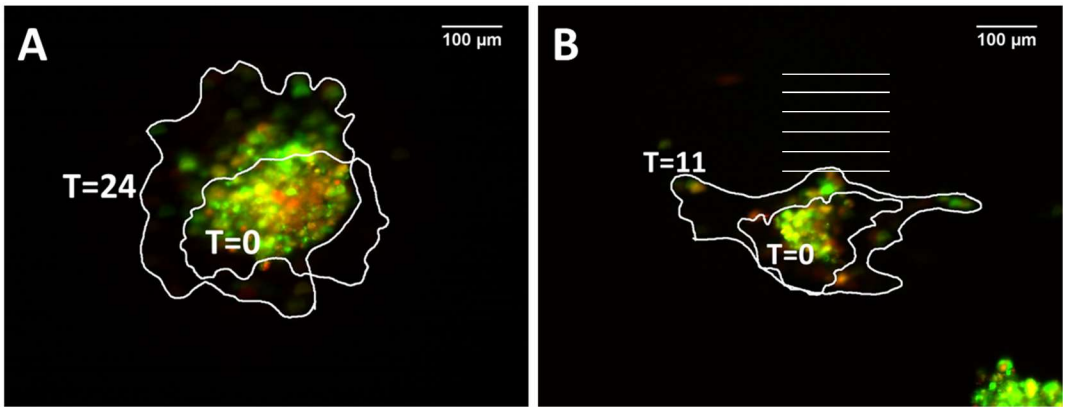

Figure 3-11: Mixed population cluster migration. Represents a flat surface and (B) represents a PDMS aligned surface. KD is represented as red and WT is represented as green.

Mixed population of n=2000 clusters in a 1:1 ratio of WT and KD were seeded on TCP and PDMS arrays. There was significantly less migration due to the long time it took for the clusters to attach to flat and PDMS array surfaces. Figure 3-11A shows the mixed population cluster on a flat surface, where it is seen that WT cells are the majority of cells on the migratory edge. In 3-11B this behavior is similarly exhibited, even showing that KD cells follow the WT cell migration. Figure 3-12A shows that the directionality of mixed KD cells on the line pattern is significantly lower than KD. In 3-12B the directionality of WT cells on both flat and lines are significantly higher than the mixed WT comparison on each pattern respectively.

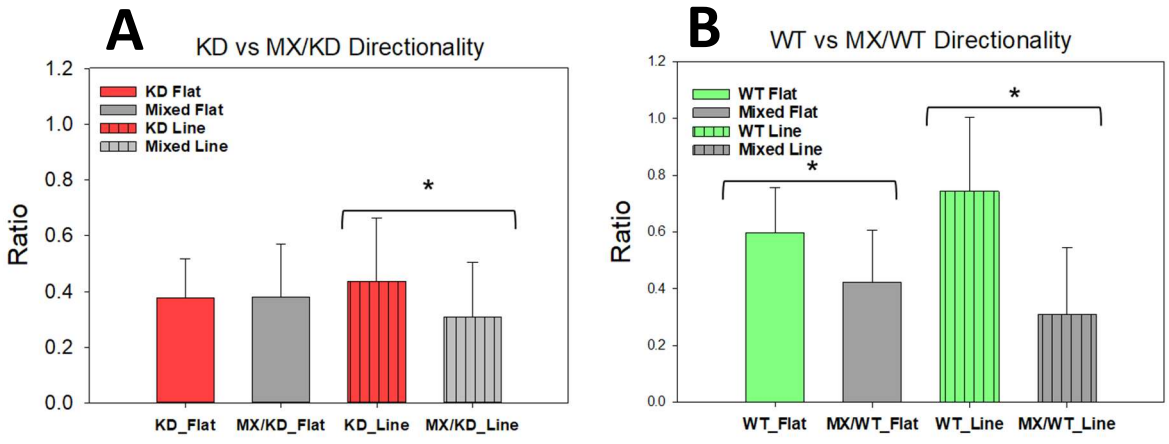

Figure 3-12: Directionality analysis of KD and WT mixed populations. Represents the directionality of KD cells and (B) represents the directionality of WT cells where only the same surface condition were compared (*$p<0.05$).

3.7 Decreasing Aligned PA Gel Stiffness Significantly Decreased Migration

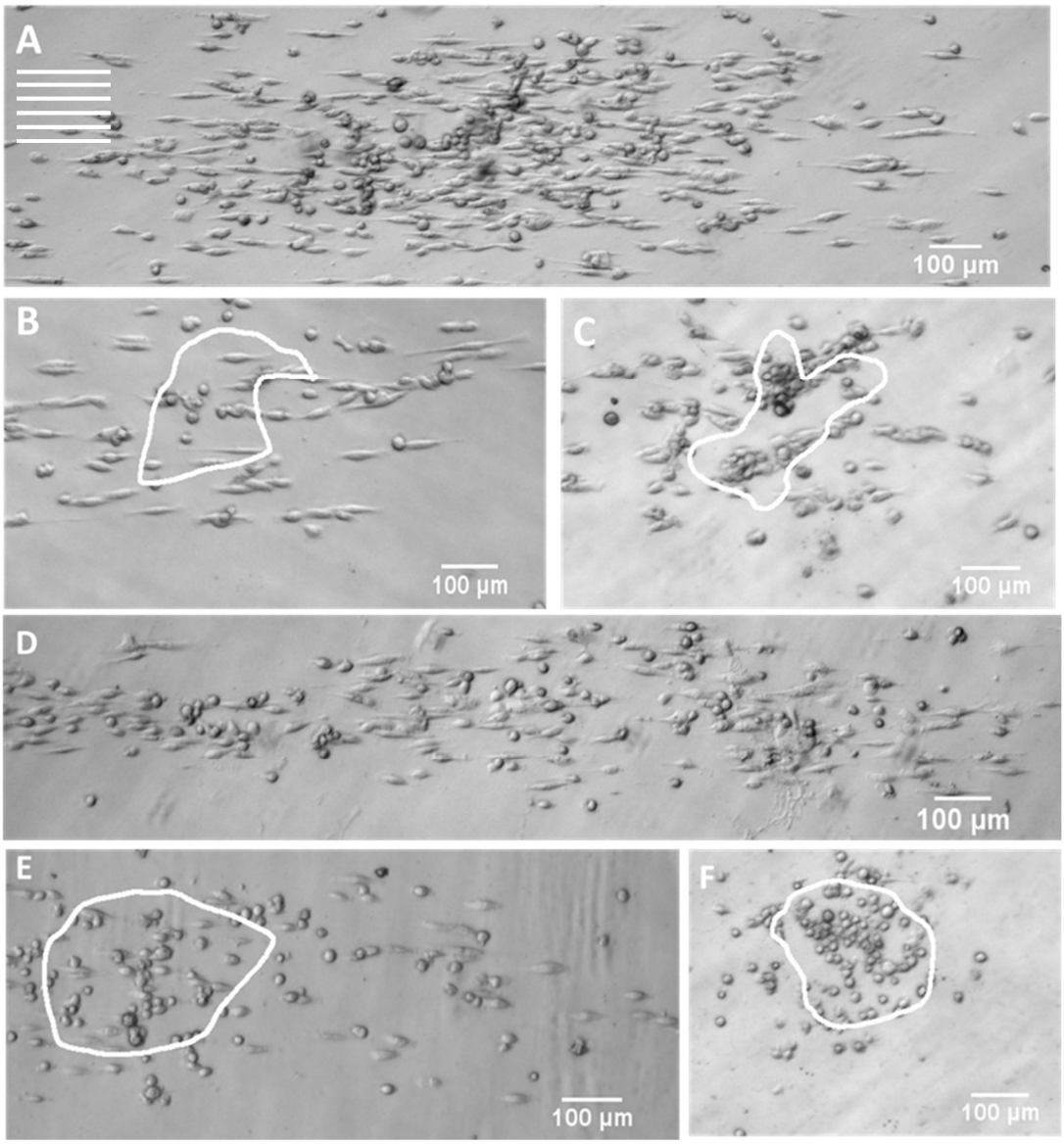

Figure 3-13: KD and WT migration on varying lined gel stiffness. All gels have lined patterns in the x-axis. (A-C) represents KD cells and (D-F) represent WT. (A) and (D) are 20 kPa, (B) and (E) are at 2 kPa, (C) and (F) are at 0.5 kPa. The highlighted white portions show the initial cluster, (A) and (D) do not have these because the migration began before a initial cluster could be observed.

In Figure 3-13, A-C represent the KD clusters and D-F represent WT. The highest gel stiffness (20 kPa) of both KD (3-13A) and WT(3-13D) show almost indistinguishable

morphology. This is also present for both cell lines on the 2kPa gels. But on 0.5 kPa gels it is clearly seen that KD cells (3-13C) attain a mesenchymal structure but WT cells (3-13F) become more epithelial like and migrate less.

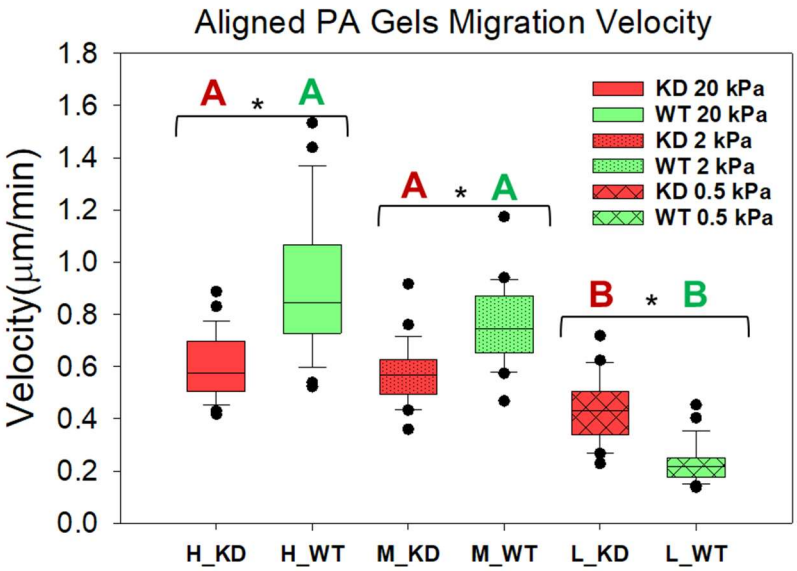

Figure 3-14: Analysis of varying gel stiffness on KD and WT. KD and WT cell clusters were seeded on 0.5 kPa. 2 kPa and 20 kPa lined PA gels (*$p<0.05$). The red letters represent KD and the green letters represent WT, where different letters show a statistical significance ($p<0.05$).

In Figure 3-14, comparing the KD clusters on various stiffnesses, it is seen that 20 kPa and 2 kPa do not show a difference in velocity, but 0.5 kPa shows a statistically lower difference. These results were also seen in the WT clusters. When comparing WT and KD on each gel stiffness, WT were significantly faster on 20 kPa and 2 kPa gels. But interestingly, on the 0.5 kPa gel, the WT showed a significantly lower velocity than KD cells.

Chapter 4 : Discussion and Conclusion

The purpose of this study was to continue to explore the effects of knocking-down myoferlin on migration of invasive breast cancer cells. The triple-negative cell line, MDA-MB-231, was used because of its overexpression of myoferlin (Li et al., 2012). Triple-negative cell lines lack HER-2, PR, and ER receptors for hormonal therapy, therefore an alternative approach to prevent a tumor from metastasizing must be found (Bianchini et al., 2016). This study focused on two aspects of the TME, collagen crosslinking and matrix stiffness. It is known that as a tumor is becoming malignant, collagen matrix crosslinking occurs around the tumor (Levental et al., 2009). During this process, the collagen matrix becomes more aligned and the matrix begins to stiffen. This is associated with the degradation of the basement membrane, which contributes to proliferation and tumorigenesis (Bilder et al., 2000). These invasive cells then utilize the stiff and aligned matrix to migrate and eventually metastasize (Bissell & Radisky, 2001). Knocking-down myoferlin has been proven to induce MET, therefore this study will test how advantageous it is to target the process of EMT to stop tumor migration (Li et al., 2012).

First, a wound closure assay was performed. It was found that KD cells have a lowered velocity compared to LVC and WT, while the directionality of each cell line was not statistically significant. Previous studies found similar results, that KD had a lower migration velocity but also found that KD had a higher directionality (Volakis et al., 2014). Since this study only had an n=25, more experiments should be performed to confirm any conclusions. Additionally, a mixed population in equal amounts of WT and KD were used in the wound assay. Interestingly, the mixed population KD had a higher velocity than isolated KD. It was observed that WT cells tended to leave the migration front and lead migration. As this occurred, KD cells tended to follow the migration of WT cells. A similar process is known that CAFs promote invasion by

generating ECM for cancer cells to travel on (Gaggioli et al., 2007). In this case, because WT cells are known to be stiffer, and have an elongated morphology with aligned actin stress fibers, they may be able to guide the KD cells (Volakis et al., 2014).

The next experiment focused on single front migration that mimicked stiff matrix crosslinking with an aligned PDMS array. Velocity and x-axis velocity where used to quantify overall migration and x-axis directed migration respectively. In terms of Velocity, LVC cells exhibited a significant increase on parallel and perpendicular array compared to a flat surface and similar results were found for KD. When comparing KD to LVC, it was confirmed that LVC travel faster on flat surfaces, but there was no difference in migration on parallel and perpendicular arrays. This potentially indicates that a stiff and aligned collagen matrix could induce EMT in KD cells. A western blot testing EMT markers such as E-cad, where cells are cultured on the PDMS array should be further studied to confirm this hypothesis. When reviewing x-axis velocity, LVC cells expressed greatest migration on the perpendicular array, following was the flat surface, and the lowest was on the parallel array. KD cells had high x-axis velocity on the perpendicular pattern but had similar velocities on parallel and flat surfaces. Interestingly, KD cells had a higher x-axis velocity on the parallel array then the LVC cells. LVC cells have been shown to have a higher traction stress then KD and as previously stated have a greater alignment of stress action formation (Volakis et al., 2014). Due to the properties of the LVC cell, there may be stronger attachment to the parallel array causing less migration. KD cells are more epithelial, therefore they do not express the same amount of focal adhesion forces as LVC. Additionally, KD cells are known to migrate in a sheet like fashion due to the expression of E-cad (Li et al., 2012). Since there is also less surface area for the cells to attach to, this could help aid migration in the x-direction. A mixed cell population experiment was also repeated for

the single front migration assay. Interestingly, both mixed WT and KD had a lower velocity than their isolated version on the parallel array. Since each cell line has a preference of migrating along the lined pattern, there may be a competitive behavior between both the cell lines. Since KD are more epithelial, they are able to spread more along a surface (Volakis et al., 2014). In this case WT cells may need to compete for adhesion. It is possible that due to competition, each cell line migrates slower and since WT are more stiff and spread less (Volakis et al., 2014), they in particular could attach at a lower rate and potentially slow down KD migration due to blocking. Additionally, the velocity of mixed KD was lower on the perpendicular array as well which could also be explained by the potential of WT cells blocking the KD migration.

The cluster migration experiment was performed on flat and PDMS aligned arrays as well, but clusters of size n=2000 were seeded on each surface. The velocity and directionality were quantified to calculate overall migration. In terms of velocity, both KD and LVC were significantly faster on the aligned surface than on the flat surface. But KD interestingly showed a faster migration velocity than LVC on the line pattern. This contradicts the idea that KD cells show more epithelial like behavior having more cell-cell adhesion. The lined pattern clearly negates the purpose of knock-down myoferlin, which possibly could be due to KD cells abilities to spread more than LVC. In terms of directionality, LVC was more directional on the lined pattern, while KD did not have a difference. Since it was seen that KD cells migrate more significantly adjacent of the PDMS array (shown in the single front migration on the parallel array), this could explain such behavior. LVC and KD on flat surfaces did not have a difference in directionality, while LVC had a significantly higher directionality on the lined surface. This is potentially due to LVC having a more aligned actin structure, and therefore the lined pattern promotes even more directionality in the direction of the elongated pattern. For the mixed

population experiments directionality was analyzed. KD did not see a difference on the flat surface, but on the lined pattern, the mixed population showed a lower directionality. This behavior is seen similarly on the lined patterns of the single front migration experiment, therefore the competition and blocking hypothesis could apply here as well. For WT, the mixed population directionality was significantly lower on both flat and aligned pattern surfaces. Again, a similar hypothesis as stated previously could explain this behavior.

The purpose of the aligned polyacrylamide gel with various gel stiffness was used to see the effect of changing the aligned matrix stiffness on migration velocity. The elastic modulus of normal breast tissue has an elastic modulus of 0.4 – 2kPa while cancerous breast tissue is around 4-12kPa (Yu et al., 2011). Therefore, 20 kPa, 2 kPa and 0.5 kPa gels were used to mimic the range of normal and tumor stroma. For KD, there was no difference between 20 kPa and 2kPa gels, but the 0.5 kPa gel was significantly slower. Previous studies showed that there is no difference in KD migration distance was found between 20 kPa, 2 kPa and 0.5 kPa gels on a flat surface (Watts & Ghadiali, 2017). Therefore, it is seen that an aligned pattern significantly effects KD migration between the range of 0.5 kPa and 2kPa. For WT, there was no difference between 20 kPa and 2kPa gels, but the 0.5 kPa gel was significantly slower. Previous studies showed that all gel migration was significantly different, where the highest stiffness gel had the most migration on the flat surface (Watts & Ghadiali, 2017). It can be concluded that an aligned matrix does increase migration when there is a high stiffness (above 2 kPa). When comparing WT and KD on each gel stiffness, WT were significantly faster on 20 kPa and 2 kPa gels, which shows the same results as experiments done on flat gel surfaces (Watts & Ghadiali, 2017). But interestingly, on the 0.5 kPa gel, the WT showed a significantly lower velocity than KD cells. Previous studies showed that on 0.5 kPa gels, LVC seemed to migrate slower initially than KD

cells, but eventually began to migrate at the same rate after 24 hours, but no statistical significance was found between the migratory patterns (Watts & Ghadiali, 2017). Therefore, it can be concluded that the soft (0.5 kPa) aligned matrix prevents WT/LVC cells from migrating. Since LVC cells have a higher traction force (Volakis et al., 2014), when they begin to migrate on the soft gel, the gel may be deforming, preventing the cells from migrating. To test this hypothesis a TFM experiment on the aligned gels should be performed.

Overall it can be concluded that an aligned matrix does assist migration velocity in both MYOF-KD and WT cells. On the PDMS arrays, there seems to be no difference in migratory velocity of LVC and KD cells. But in the cluster experiments there is contradictory results which could indicate that a single front migration assay and a cluster assay model different tumor behavior. When stiffness is introduced, it is seen that on higher stiffness gels, MYOF-KD does migrate slower, but interestingly on the lowest stiffness gel WT cells migrate the slowest. Mixed populations of KD and WT cells were also studied to see if partial knock down of a cell population is effective. Interestingly on the wound assay, mixing populations increases migration, while in single front and cluster experiments it lowered migratory abilities, which indicates that a two front migration improves migration possibly due to chemotaxis. Additional studies should be done exploring the migratory behavior of knocking down myoferlin through TFM. Additionally, western blots should be performed to see if an aligned matrix promotes upregulation of MET markers in the MYOF-KD.

References

@NCICancerStats. (2019). SEER Cancer Statistics Review, 1975-2015.

Argon, Y., & Ward, S. (1980). Caenorhabditis elegans fertilization-defective mutants with abnormal sperm. *Genetics, 96*(2), 413-433.

Bansal, D., & Campbell, K. P. (2004). Dysferlin and the plasma membrane repair in muscular dystrophy. *Trends Cell Biol, 14*(4), 206-213. doi:10.1016/j.tcb.2004.03.001

Barnhouse, V. R., Weist, J. L., Shukla, V. C., Ghadiali, S. N., Kniss, D. A., & Leight, J. L. (2018). Myoferlin regulates epithelial cancer cell plasticity and migration through autocrine TGF-beta1 signaling. *Oncotarget, 9*(27), 19209-19222. doi:10.18632/oncotarget.24971

Bianchini, G., Balko, J. M., Mayer, I. A., Sanders, M. E., & Gianni, L. (2016). Triple-negative breast cancer: challenges and opportunities of a heterogeneous disease. *Nat Rev Clin Oncol, 13*(11), 674-690. doi:10.1038/nrclinonc.2016.66

Bilder, D., Li, M., & Perrimon, N. (2000). Cooperative regulation of cell polarity and growth by Drosophila tumor suppressors. *Science, 289*(5476), 113-116.

Bissell, M. J., & Radisky, D. (2001). PUTTING TUMOURS IN CONTEXT. *Nat Rev Cancer, 1*(1), 46-54. doi:10.1038/35094059

Bonotto, M., Gerratana, L., Poletto, E., Driol, P., Giangreco, M., Russo, S., . . . Puglisi, F. (2014). Measures of Outcome in Metastatic Breast Cancer: Insights From a Real-World Scenario. In *Oncologist* (Vol. 19, pp. 608-615).

Brabletz, T., Kalluri, R., Nieto, M. A., & Weinberg, R. A. (2018). EMT in cancer. *Nature Reviews Cancer, 18*(2), 128. doi:doi:10.1038/nrc.2017.118

Breastcancer.org - Breast Cancer Information and Support. (2019).

Cox, T. R., & Erler, J. T. (2011). Remodeling and homeostasis of the extracellular matrix: implications for fibrotic diseases and cancer. In *Dis Model Mech* (Vol. 4, pp. 165-178).

Dvorak, H. F., Flier, J. S., & Underhill, L. H. (2009). Tumors: Wounds That Do Not Heal. *http://dx.doi.org.proxy.lib.ohio-state.edu/10.1056/NEJM198612253152606*. doi:NJ198612253152606

Flanders, K. C., & Wakefield, L. M. (2009). Transforming growth factor-βs and mammary gland involution; functional roles and implications for cancer progression. *J Mammary Gland Biol Neoplasia, 14*(2), 131-144. doi:10.1007/s10911-009-9122-z

Gaggioli, C., Hooper, S., Hidalgo-Carcedo, C., Grosse, R., Marshall, J. F., Harrington, K., & Sahai, E. (2007). Fibroblast-led collective invasion of carcinoma cells with differing roles for RhoGTPases in leading and following cells. *Nature Cell Biology, 9*(12), 1392. doi:doi:10.1038/ncb1658

Hu, M., Yao, J., Cai, L., Bachman, K. E., Brûle, F. v. d., Velculescu, V., & Polyak, K. (2005). Distinct epigenetic changes in the stromal cells of breast cancers. *Nature Genetics, 37*(8), 899. doi:doi:10.1038/ng1596

Kalluri, R. (2016). The biology and function of fibroblasts in cancer. *Nat Rev Cancer, 16*(9), 582-598. doi:10.1038/nrc.2016.73

Kalluri, R., & Weinberg, R. A. (2009). The basics of epithelial-mesenchymal transition. In *J Clin Invest* (Vol. 119, pp. 1420-1428).

Levental, K. R., Yu, H., Kass, L., Lakins, J. N., Egeblad, M., Erler, J. T., . . . Weaver, V. M. (2009). Matrix crosslinking forces tumor progression by enhancing integrin signaling. *Cell, 139*(5), 891-906. doi:10.1016/j.cell.2009.10.027

Li, R., Ackerman, W. E., Mihai, C., Volakis, L. I., Ghadiali, S., & Kniss, D. A. (2012). Myoferlin Depletion in Breast Cancer Cells Promotes Mesenchymal to Epithelial Shape Change and Stalls Invasion. In *PLoS One* (Vol. 7).

Miller, C., & Hansford, D. (2018). Cells on Gels: Micron-scale polyacrylamide gels for studies of glioblastoma multiforme cell adhesion, morphology, and migration. doi:http://hdl.handle.net/1811/84587

NBCF. (2019). Information, Awareness & Donations :: The National Breast Cancer Foundation.

Paszek, M. J., Zahir, N., Johnson, K. R., Lakins, J. N., Rozenberg, G. I., Gefen, A., . . . Weaver, V. M. (2005). Tensional homeostasis and the malignant phenotype. *Cancer Cell, 8*(3), 241-254. doi:10.1016/j.ccr.2005.08.010

Peinado, H., Quintanilla, M., & Cano, A. (2003). Transforming growth factor beta-1 induces snail transcription factor in epithelial cell lines: mechanisms for epithelial mesenchymal transitions. *J Biol Chem, 278*(23), 21113-21123. doi:10.1074/jbc.M211304200

Rittweger, J., Simunic, B., Bilancio, G., De Santo, N. G., Cirillo, M., Biolo, G., . . . Narici, M. (2009). Bone loss in the lower leg during 35 days of bed rest is predominantly from the cortical compartment. *Bone, 44*(4), 612-618. doi:10.1016/j.bone.2009.01.001

Ronnov-Jessen, L., & Petersen, O. W. (1993). Induction of alpha-smooth muscle actin by transforming growth factor-beta 1 in quiescent human breast gland fibroblasts. Implications for myofibroblast generation in breast neoplasia. *Lab Invest, 68*(6), 696-707.

Roux, I., Safieddine, S., Nouvian, R., Grati, M., Simmler, M. C., Bahloul, A., . . . Petit, C. (2006). Otoferlin, defective in a human deafness form, is essential for exocytosis at the auditory ribbon synapse. *Cell, 127*(2), 277-289. doi:10.1016/j.cell.2006.08.040

Rønnov-Jessen, L., Petersen, O. W., Koteliansky, V. E., & Bissell, M. J. (1995). The origin of the myofibroblasts in breast cancer. Recapitulation of tumor environment in culture unravels diversity and implicates converted fibroblasts and recruited smooth muscle cells. *J Clin Invest, 95*(2), 859-873.

Shukla, V. C., Higuita-Castro, N., Nana-Sinkam, P., & Ghadiali, S. N. (2016). Substrate stiffness modulates lung cancer cell migration but not epithelial to mesenchymal transition. *J Biomed Mater Res A, 104*(5), 1182-1193. doi:10.1002/jbm.a.35655

Sternlicht, M. D., Lochter, A., Sympson, C. J., Huey, B., Rougier, J. P., Gray, J. W., . . . Werb, Z. (1999). The stromal proteinase MMP3/stromelysin-1 promotes mammary carcinogenesis. *Cell, 98*(2), 137-146.

Termine, J. D., Belcourt, A. B., Conn, K. M., & Kleinman, H. K. (1981). Mineral and collagen-binding proteins of fetal calf bone. *J Biol Chem, 256*(20), 10403-10408.

Tse, J. R., & Engler, A. J. (2010). Preparation of hydrogel substrates with tunable mechanical properties. *Curr Protoc Cell Biol, Chapter 10*, Unit 10.16. doi:10.1002/0471143030.cb1016s47

Volakis, L. I., Li, R., Ackerman, W. E., Mihai, C., Bechel, M., Summerfield, T. L., . . . Kniss, D. A. (2014). Loss of Myoferlin Redirects Breast Cancer Cell Motility towards Collective Migration. In *PLoS One* (Vol. 9).

Watts, K., & Ghadiali, S. (2017). Influence of Tumor Microenvironment Biophysical Properties on Myoferlin-Mediated Changes in Breast Cancer Cell Migration and Invasion. doi:http://hdl.handle.net/1811/80458

Wipff, P. J., Rifkin, D. B., Meister, J. J., & Hinz, B. (2007). Myofibroblast contraction activates latent TGF-β1 from the extracellular matrix. In *J Cell Biol* (Vol. 179, pp. 1311-1323).

Yu, H., Mouw, J. K., & Weaver, V. M. (2011). Forcing form and function: biomechanical regulation of tumor evolution. *Trends Cell Biol, 21*(1), 47-56. doi:10.1016/j.tcb.2010.08.015

Zeisberg, M., Shah, A. A., & Kalluri, R. (2005). Bone morphogenic protein-7 induces mesenchymal to epithelial transition in adult renal fibroblasts and facilitates regeneration of injured kidney. *J Biol Chem, 280*(9), 8094-8100. doi:10.1074/jbc.M413102200